Journal of the Physical Society of Japan
Vol. 79, No. 4, April, 2010, 044712

Microscopic Study of Dendritic Avalanches in MgB_2 Thin Films of Various Widths

Jae-Yeap LEE, Hyun-Sook LEE, Hu-Jong LEE, Eun-Mi CHOI[1], Won-Nam KANG[1], and Sung-Ik LEE[2*]

National Creative Research Initiative Center for Superconductivity, Department of Physics, Pohang University of Science and Technology, Pohang 790-784, Korea
[1]*BK21 Division and Department of Physics, Sungkyunkwan University, Suwon 440-746, Korea*
[2]*National Creative Research Initiative Center for Superconductivity, Department of Physics, Sogang University, Seoul 121-742, Korea*

(Received September 22, 2009; accepted February 22, 2010; published April 12, 2010)

To understand the features of a dendritic avalanche, we prepared the eight sets of MgB_2 thin films with rectangular shapes of 3 mm [length L] $\times$ w [width], where $w = 0.2$ to 1.6 mm; the samples were in the long-length limit of $w < L$. Magneto-optical images (MOIs) of the first few dendrite patterns, which were distributed sparsely, were taken at applied fields below 35 mT at a temperature of 4 K. The key features of the present measurements are as follows: (1) the number of branches and the area of the dendrites increase with increasing w; (2) the change in the flux density (CFD) from before to after the jump at the edge of the samples increased with increasing w; (3) the applied magnetic flux density of the first few appearances of dendrites decreased with increasing of the w; (4) the real initial penetration flux density at the sample's edge was about 20 mT, regardless of w; (5) the critical current densities obtained from the MOI were almost the same for all samples, which implies that Bean's critical model works quite well.

KEYWORDS: MgB_2 thin film, flux jump, demannetization effect
DOI: 10.1143/JPSJ.79.044712

1. Introduction

The origin of a vortex avalanche propagating with a dendritic shape is known to be a thermo-magnetic instability triggered by the positive feedback of continuously penetrating vortices.[1–5] This interesting phenomenon takes place in some superconducting films, like Nb, Nb alloys, and $YBa_2Cu_3O_x$,[6–9] especially at low temperatures and low magnetic fields. In addition to the above materials, a stronger dendrite appears in MgB_2 thin films because of the higher Joule heating generated by the coupling between the high critical current density (J_c) and the induced electric field. In addition, magnetic and thermal diffusion play key roles in a dendritic avalanche. Theoretically, when magnetic diffusion is much higher than thermal diffusion, a superconducting thin film becomes thermally unstable.[10,11] In fact, a dendritic avalanche can be studied by investigating magnetic hysteresis loops and by using a magneto-optical (MO) imaging method.[11–16] Magnetic hysteresis loops show macroscopic magnetic signal over a wide range of magnetic field, but MOI shows the microscopic behavior of a vortex avalanche over a limited range of magnetic fields.

A number of works have been done in an effort to understand this phenomenon.[1–11] One way to control a dendritic avalanche is by increasing heat diffusion. Once a large amount of the heat in a MgB_2 thin film is transferred to a heat reservoir, like a metal layer on top of the superconducting film, the dendritic avalanche is suppressed.[12–14] Another way to control a vortex avalanche is by changing the demagnetization factor.[11,14,15] Dendrite formation critically depends on the width (w) of the MgB_2 thin films, and this phenomenon has been well confirmed to disappear below a threshold w because of the demagnetization effect. Even though research on this subject has been previously reported, still a detailed study of the impact of the demagnetization effect on the appearance of a vortex avalanche is needed if this phenomenon is to be understood.

To study the demagnetization effect in microscopic level, we used the MOI method. For the first step, we examined the critical current density obtained by using Bean's critical state model while using MOIs to analyze the flux profiles. We found that the obtained critical current densities were about 6×10^6 A/cm^2, regardless of the sample's width, which means that this model works quite well and that the patterning does not degrade the MgB_2 thin films. We also obtained several other results, which will be discussed below, that allowed us to conclude that the various avalanche behaviors observed for different value of w were, indeed, related to the demagnetization effect.

2. Experiments and Discussion

We synthesized MgB_2 thin films by using a two-step method composed of pulsed laser deposition (PLD) and post annealing. A boron precursor film was deposited on a sapphire substrate by using a PLD system; then, the sample was put into Nb tube with pure Mg metal. In this procedure, possible contamination of the samples was blocked because the sample was not exposed to the air. The superconducting transition temperature, which was confirmed by using the magnetization curve, was 39 K. The details of the synthesis are presented in ref. 17. To make thin films with different values of w, we patterned eight films, by using photolithography, with different rectangular shapes on the same substrate. The films had values of w ranging from 0.2 to 1.6 mm for a given length of 3 mm, which indicates that most of the thin films fell within the long-length limit, so

*E-mail: silee77@sogang.ac.kr

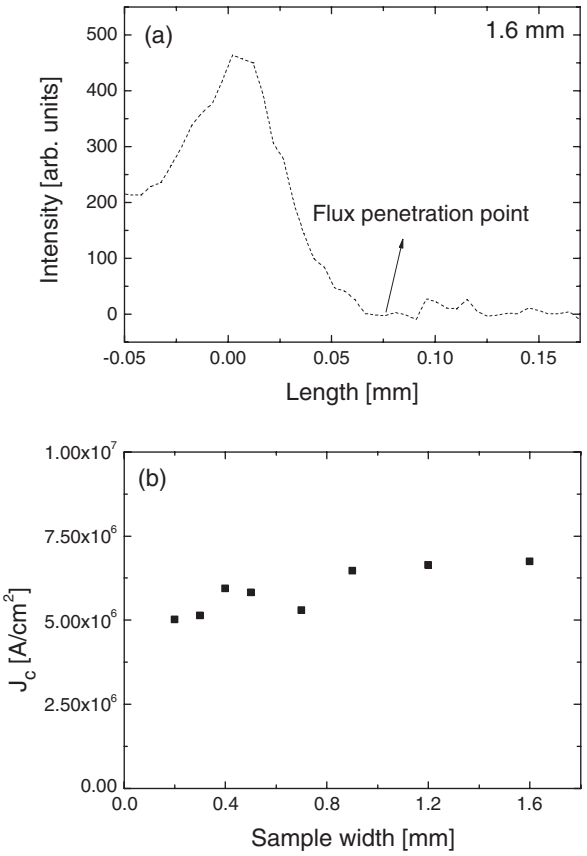

Fig. 1. (a) Flux profile obtained at the edge of a 1.6-mm-wide sample. The black arrow indicates the flux penetration depth from the edge, and zero on the horizontal axis means the edge of the sample. (b) Values of J_c for the eight samples.

dendritic propagation mainly appeared from the long edge to the center of sample. We chose a MOI method[18] to investigate the microscopic features of dendritic propagation in MgB_2 thin films with various value of w for magnetic fields up to 35 mT at 4 K. In this magnetic field and temperature range, we could use MOIs of sparsely distributed dendrites without overlap.

To determine the quality of each patterned thin film and the validity of using Bean's critical state model to find the critical current densities, we calculated the critical current density, J_c, from the MOI data. Bean's model tell us that J_c can be expressed in terms of the flux penetration depth (δ), which can be directly obtained from the MOI profile near the edge of sample.[19–21] The intensity profile of $w = 1.6$ mm and the flux penetration depth for that width which an intensity value goes to zero are shown in Fig. 1(a). At small fields, the J_c based on Bean's critical state model is given by

$$\delta = \sqrt{\frac{0.5w}{\delta}}\frac{\pi B_a}{\mu_0 d} \quad (1)$$

where w is a half width of the sample (half of 0.2 to 1.6 mm) and thickness, $d = 300$ nm. The applied magnetic field, B_a, was 4.9 mT. As shown in Fig. 1(b), the J_c for different w does not change much, which implies that micro-patterning does not degrade the sample's quality and that Bean's critical state model works quite well in these MgB_2 thin films.

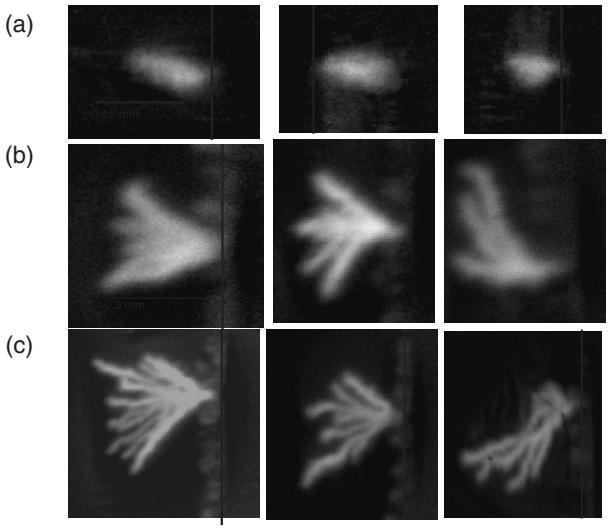

Fig. 2. Magneto-optical images of dendritic branches appearing in the (a) 0.3-, (b) 0.7-, and (c) 1.6-mm samples.

Figure 2 shows MOI results for the microscopic structures of the dendritic propagation. The features of a dendritic branch can be seen for $w = 0.3$, 0.7, and 1.6 mm. In this study, we chose the first seven dendrites of each sample for microscopic analysis. In this limit, dendrites distribute very sparsely, and the interactions between dendrites are negligible. In our long-length limit, dendrites appeared mostly from the long edge. As w became smaller, the shape of the dendritic structure became simpler, and finally, the branches merged to one for the 0.3-mm sample. The area of each dendrite also decreased with decreasing w. In Fig. 3, we draw the number of branches and their areas for the first seventh dendrites appearing for each w. The number of branches and their areas tend to decrease with decreasing of w. However, even though the applied magnetic field is increased, the shape of the dendritic structures (the number of branches and areas) for the first seven dendrites in the same sample (same w) are almost identical.

Then why shapes of the dendrites are different for the different width of the samples even though the real magnetic fields of the first few penetration are same? Actually, the vortex avalanche is originated from the thermo-magnetic instability triggered by the positive feedback of continuously penetrating vortices. In this case, a small change of the initial conditions could generate huge differences of vortex propagation. For the sample of the wider width with the large demagnetization factor, the vortex invasion into the thin film is easier due to the existence of large empty vortex free area. This can make vortices diffused into the thin film faster for the wider sample and generates a much amplified Joule heating which is proportional to $J \times E$ ($E \sim dH/dT$). This may be the reason why much more complex shape of the avalanche appears for the sample with large width as shown in MOI.

We also investigated the w dependence of the change in the flux density (CFD). When a dendrite appears, the real flux density at the edge is reduced by a certain amount. While many vortices flow into the thin film within a very short time interval, the size of the dendritic jump and the CFD could be obtained from the MO images. Figure 4(a)

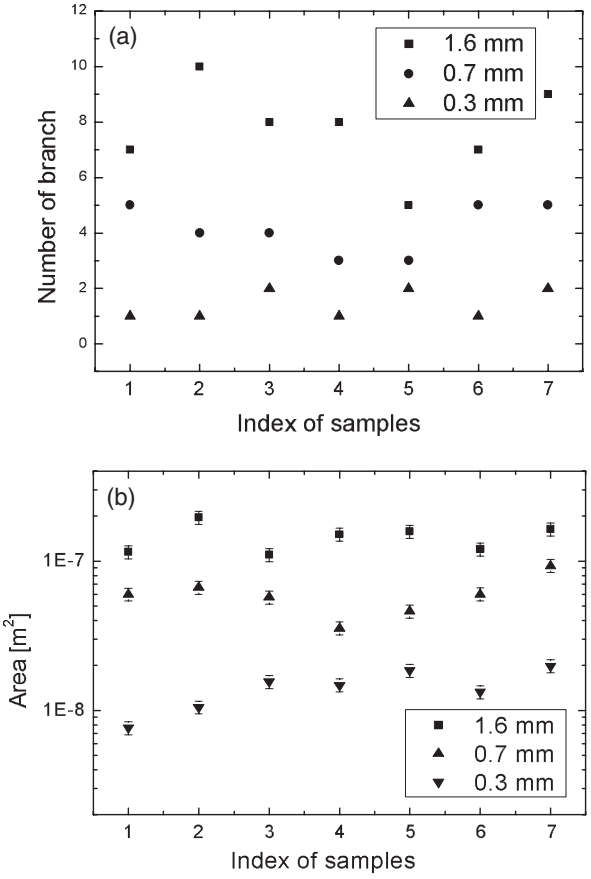

Fig. 3. (a) Number of branches and (b) their areas for $w = 0.3$, 0.7, and 1.6 mm. The numbers on the horizontal axis represent the seven investigated dendrites.

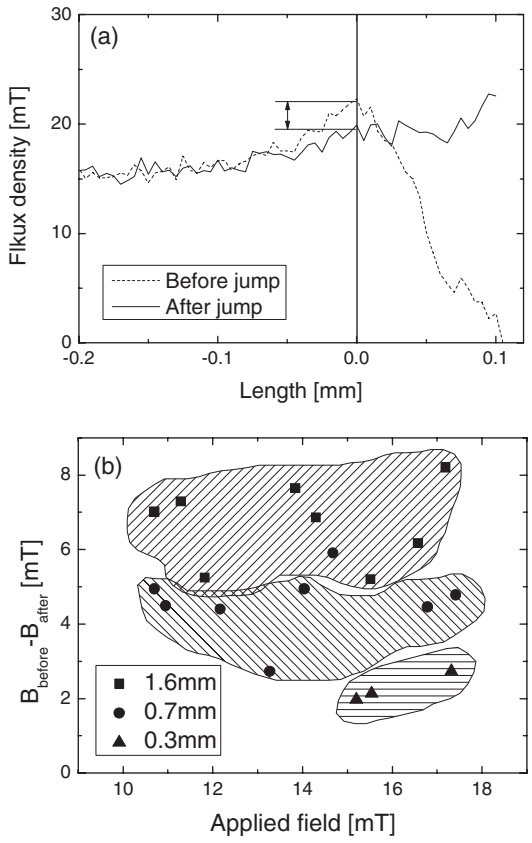

Fig. 4. (a) Flux density just before and after the appearance of an avalanche for $w = 0.3$ mm. (b) Distributions of the CFD for $w = 1.6$, 0.7, and 0.2 mm.

shows profiles of the flux density obtained from MOI just before and after the appearance of an avalanche for $w = 0.3$ mm. Figure 4(b) shows the distributions of the CFD for $w = 1.6$, 0.7, and 0.3 mm for $10 < H < 18$ mT. In this field range, dendrites do not interact with each other because only a few dendrites appear. For $w = 1.6$ mm (0.7 mm), the CFD varies from 5.2 to 8.2 mT (2.7–5.9 mT), and for $w = 0.3$ mm, the distribution of the CFD is 1.9–2.7 mT. Curiously enough, the CFD does not change much as long as w remains the same. The result in Fig. 2 can be explained in the same way. Because a larger CFD means that many vortices penetrate into the sample, the area and the number of branch are the largest for $w = 1.6$ mm sample as shown in Fig. 3.

Now, we would like to analyze the w dependence of the dendritic jump in more detail. We noticed that their shapes, number of branch or areas and the CFD do not much depend very much on the applied magnetic field as long as w is same. However, when w is changed, these quantities also change. The change in the CFD for different value of w causes the areas, number of branches, and, thus, the shapes of the dendrites to be different.

In Fig. 5, we present the real magnetic flux density for the first three dendritic jumps at the edges of the samples just before the jump for different values of w as obtained from the MO images. The demagnetization is known to have a significant effect on these jumps, and for different w, the magnetic field of the first flux jump at the edge of the thin film is different. However, we expect to have almost the same real magnetic flux density of the first dendritic penetration (B_P) for the flux jump. As expected, the value of B_P, which has never been measured before as a function of w, turns out to be about the same, about 20 mT. We also found that the local real flux densities just before the second and the third jumps were also almost the same for different value of w. Thus, one can infer that the local flux density at the edge must exceed a certain value, as mentioned above, for dendritic propagation to occur. This experimental observation can be explained in the following way. When w is small, a dendritic jump cannot appear easily because the local magnetic flux density at the edge is not very much larger than the applied magnetic field due to the small demagnetization effect. Thus, dendritic propagation hardly appears in a narrow sample. For large w, on the other hand, the flux density at the edge of the thin film is much enhanced due to the demagnetization effect, so a high applied magnetic field is not needed for a dendritic jump to occur.

3. Summary and Conclusions

It is important to know how the physical quantities in a vortex avalanche depend on the demagnetization. For this purpose, we used the MO imaging method to conduct a detailed microscopic detailed study on the impact of the demagnetization effect on dendritic avalanches in various sizes of MgB_2 thin films of various sizes. The J_c obtained by using Bean's critical state model had almost the same value, regardless of the w, which confirmed the validity of the above model and demonstrated that the thin films has not

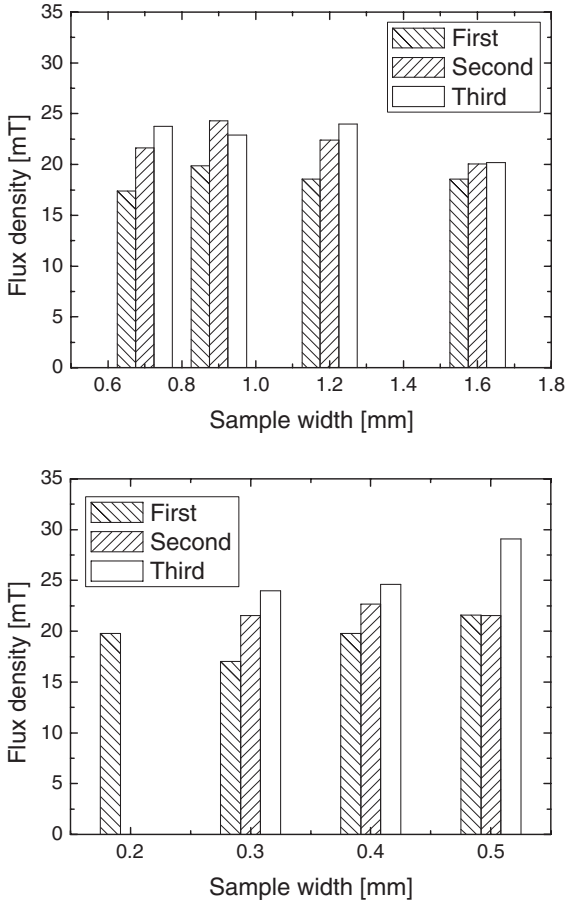

Fig. 5. Flux density obtained at the edge of the sample before the occurrence for the first three dendritic jumps.

been degraded during the micro-patterning. The CFD before and after the avalanche at the edge of the thin film, the number of branches, and the area of each dendrite critically depend on w. However, for a given value of w, the local magnetic flux density at the edge of a thin film just before the first to the third appearance of a dendrite was found to be about the same even though the applied magnetic field has changed. Also the highly diversified shape of the avalanche appears for the sample with larger width due to the highly amplified Joule heating even though real fields at the edge of the samples for the vortex avalanche are same. Thus, we can conclude that a vortex avalanche is, indeed, related to the demagnetization effect and that it critically depends on the sample width, but the local magnetic flux density for the appearance of the first few dendrites does not depend on the sample's width.

Acknowledgments

This work was supported by the Center for Superconductivity of the program of Acceleration Research of MOST/KOSEF of Korea and by a special fund of Sogang University.

1) T. H. Johansen, M. Baziljevich, D. V. Shantsev, P. E. Goa, Y. M. Galperin, W. N. Kang, H. J. Kim, E. M. Choi, M.-S. Kim, and S. I. Lee: Europhys. Lett. **59** (2002) 599.
2) P. Leiderer, J. Boneberg, P. Brüll, V. Bujok, and S. Herminghaus: Phys. Rev. Lett. **71** (1993) 2646.
3) D. V. Shantsev, A. V. Bobyl, Y. M. Galperin, T. H. Johansen, and S. I. Lee: Phys. Rev. B **72** (2005) 024541.
4) D. V. Denisov, A. L. Rakhmanov, D. V. Shantsev, Y. M. Galperin, and T. H. Johansen: Phys. Rev. B **73** (2006) 014512.
5) A. L. Rakhmanov, D. V. Shantsev, Y. M. Galperin, and T. H. Johansen: Phys. Rev. B **70** (2004) 224502.
6) I. A. Rudnev, S. V. Antonenko, D. V. Shantsev, T. H. Johansen, and A. E. Primenko: Cryogenics **43** (2003) 663.
7) S. C. Wimbush, B. Holzapfel, and Ch. Jooss: J. Appl. Phys. **96** (2004) 3589.
8) I. A. Rudnev, D. V. Shantsev, T. H. Johansen, and A. E. Primenko: Appl. Phys. Lett. **87** (2005) 042502.
9) J.-Y. Lee, E.-M. Choi, H.-S. Lee, M.-H. Cho, A. A. F. Olsen, T. H. Johansen, Y. S. Oh, K.-H. Kim, Y.-H. Han, T. H. Sung, and S.-I. Lee: J. Phys. Soc. Jpn. **77** (2008) 104717.
10) I. S. Aranson, A. Gurevich, M. S. Welling, R. J. Wijngaarden, V. K. Vlasko-Vlasov, V. M. Vinokur, and U. Welp: Phys. Rev. Lett. **94** (2005) 037002.
11) D. V. Denisov, D. V. Shantsev, Y. M. Galperin, E.-M. Choi, H.-S. Lee, S.-I. Lee, A. V. Bobyl, P. E. Goa, A. A. F. Olsen, and T. H. Johansen: Phys. Rev. Lett. **97** (2006) 077002.
12) E.-M. Choi, H.-S. Lee, H.-J. Kim, S.-I. Lee, H.-J. Kim, and W. N. Kang: Appl. Phys. Lett. **84** (2004) 82.
13) E.-M. Choi, H.-S. Lee, H.-J. Kim, B.-W. Kang, S.-I. Lee, A. A. F. Olsen, D. V. Shantsev, and T. H. Johansen: Appl. Phys. Lett. **87** (2005) 152501.
14) E.-M. Choi, H.-S. Lee, S.-I. Lee, A. A. F. Olsen, D. V. Shantsev, and T. H. Johansen: J. Korean Phys. Soc. **48** (2006) 1044.
15) E.-M. Choi, H.-S. Lee, J.-Y. Lee, S.-I. Lee, A. A. F. Olsen, V. V. Yurchenko, D. V. Shantsev, T. H. Johansen, H.-J. Kim, and M.-H. Cho: Appl. Phys. Lett. **91** (2007) 042507.
16) J.-Y. Lee, E.-M. Choi, H.-S. Lee, H.-J. Lee, S.-I. Lee, A. A. F. Olsen, D. V. Shantsev, and T. H. Johansen: Supercond. Sci. Technol. **21** (2008) 105021.
17) W. N. Kang, H.-J. Kim, E.-M. Choi, C. U. Jung, and S.-I. Lee: Science **292** (2001) 1521.
18) T. H. Johansen, M. Baziljevich, H. Bratsberg, Y. M. Galperin, P. E. Lindelof, Y. Shen, and P. Vase: Phys. Rev. B **54** (1996) 16264.
19) E. Zeldov, J. R. Clem, M. McElfresh, and M. Darwin: Phys. Rev. B **49** (1994) 9802.
20) E. H. Brandt and M. Indenbom: Phys. Rev. B **48** (1993) 12893.
21) F. L. Barkov, D. V. Shantsev, T. H. Johansen, P. E. Goa, W. N. Kang, H. J. Kim, E. M. Choi, and S. I. Lee: Phys. Rev. B **67** (2003) 064513.